ACS ES&T Engineering

pubs.acs.org/estengg

Article

Ground-Breaking and Safe Recycling of Hazardous Hyperaccumulators

Zhelin He, Chao Jia, Long Cheng, Fengbo Yu, Liming Sun, Litao Lin, Tao Teng, Xuan Wu, Jie Gao, Linzhi Zuo, Ting Bian, Liang Wang, Shicheng Zhang, and Xiangdong Zhu*

Cite This: *ACS EST Engg.* 2023, 3, 1966−1974

Read Online

ACCESS | Metrics & More | Article Recommendations | Supporting Information

ABSTRACT: Hyperaccumulators are annually mass-produced, which may ultimately endanger the environment and human health without an appropriate treatment. However, the current pyrolysis technique cannot achieve efficient metal removal and produces low-value materials due to its limited heating temperature and unitary operational principle. Herein, a ground-breaking flash Joule heating (FJH) was proposed to recycle a typical zinc-enriched hyperaccumulator to a profitable material (flash graphene) with a superior metal removal efficiency. The results indicate that the FJH-induced instantaneous ultrahigh temperature (∼3000 K, 20 s) promotes metal removal efficiency and graphitization of hyperaccumulators and simultaneously current exfoliates to form 3−7 layer graphene. Moreover, light spot moving and luminance fluctuation visualized by a high-speed camera confirm that metals are adequately evaporated to squirt out from the parental hyperaccumulator. Furthermore, the crystal phase inducer evokes the chlorination reaction to improve metal removal efficiency (98.6%) under less impacts on forming a graphene structure. Accordingly, flash graphene is examined by seed germination, indicating that it is environmentally safe with a few remaining metals or environmentally persistent radicals. Then, the tested graphene with a thin layer enables a more efficient photothermal conversion for solar-driven water evaporation than pyrochar. Moreover, the economic assessment indicates that profits from the FJH treatment are ∼850-fold higher than that from pyrolysis. Thus, FJH is an avant-garde recycling technique to renovate hazardous hyperaccumulators.

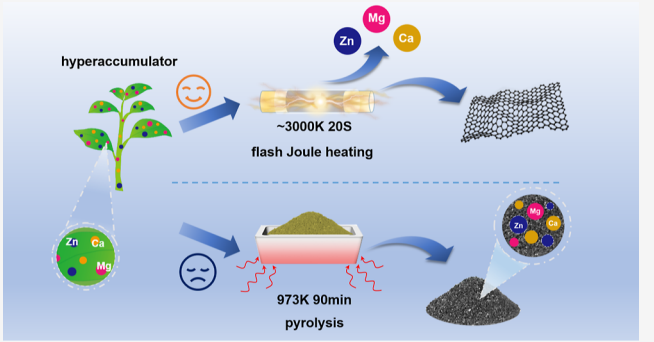

KEYWORDS: *hyperaccumulator, recycling, Joule heating, metal decontamination, pyrolysis*

1. INTRODUCTION

Hyperaccumulators, a group of plants for cost-effective environmental remediation, are annually produced in a large scale.[1−3] Notably, the abundant carbon sources in harvested plants could be reutilized to produce valuable carbon materials.[4−6] However, exposure of these carbon materials will lead to migration of endogenous metals, which may induce secondary pollution via environmental release.[7] Hence, an efficient and eco-friendly treatment is required to synchronously decontaminate and upgrade these hazardous hyperaccumulators.

Unfortunately, there are great challenges in recycling harvested hyperaccumulators. For decades of research, pyrolysis technique has been used for resource reutilization.[8−10] However, pyrolysis achieves a low metal removal efficiency due to its insufficient heating temperature and unitary operational principle.[11−13] Moreover, the produced carbon materials show limited value due to the low degree of carbonization.[14,15] Thus, these materials show inferior electron transport rate and mechanical strength, which can hinder their performance in subsequent applications, such as energy storage and material reinforcement.[16−18] Therefore, it is necessary to identify an eco-friendly method to achieve a higher metal removal efficiency and simultaneously produce more profitable materials when recycling hazardous hyperaccumulators.

Flash Joule heating (FJH), a nascent method which can upcycle biomass carbon sources to lucrative material (flash graphene), has captured significant attention.[17,19] Different from the traditional thermochemical methods, this unique technique is initiated using a current directly passed through the reactant to instantaneously drive the reactant to ultrahigh temperature (∼3000 K in 20 s).[20,21] The strong current induced high temperature accompanied by electric exfoliation, which rearranged and exfoliated the structure of the reactant to form flash graphene.[22] Since FJH-induced electric thermal

Received: July 10, 2023
Revised: October 6, 2023
Accepted: October 9, 2023
Published: October 20, 2023

https://doi.org/10.1021/acsestengg.3c00278
ACS EST Engg. 2023, 3, 1966−1974

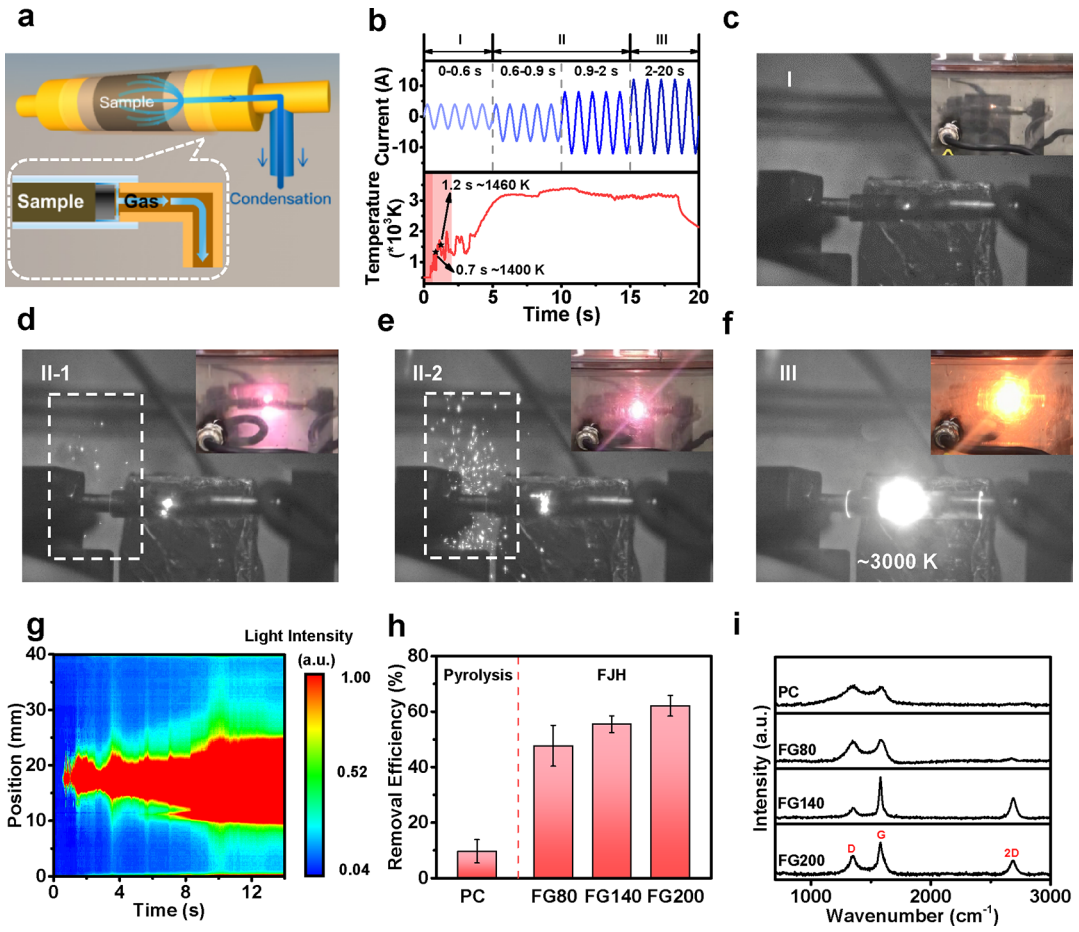

Figure 1. (a) Schematic of the FJH system. (b) Real-time temperature and current during the FJH treatment. The FJH treatment could be divided into three stages. (c–f) Real-time reacting phenomenon filmed by a high-speed camera. The inlaid images in (c–f) were the screenshots of the emitted light during the reacting process. In order to take a closer look at the reacting process, the hollow anode was replaced by a solid anode during the filming. In a typical FJH treatment, evaporated heavy metals were trapped in a collecting system. (g) Light intensity changes of different positions of the reacting sample during the FJH treatment. (h) Zn removal efficiency of the FJH treatment and pyrolysis. The error bars represent the standard deviation where each sample was tested for 2 times. (i) Raman spectra of PC and carbon materials produced by the FJH treatment.

effect provides an ultrahigh temperature over the boiling point of most metals (Figure S1), this technique has recently been applied for metal recycling.[23] Therefore, both metal recycling and material reforming rely on the ultrahigh temperature induced by FJH, implying the flexible tunability of FJH and its promising potential on renovation of hazardous hyperaccumulators. However, this promising technique has not been applied to efficiently decontaminate and upgrade hazardous hyperaccumulators.

Moreover, the crystal phase inducer has been reported that it can improve the removal of metals via chlorination reaction.[23] This is because the derived metal chlorides which have lower boiling points can be easily evaporated. However, the addition of the crystal phase inducer may elevate the resistance of the reactant, which further affects the alternating current and the electric thermal effect of FJH treatment. Nonetheless, there is little information on how the crystal phase inducer impacts graphene fabrication, which also requires further investigation.

In this study, a homemade FJH system was constructed, and a typical hyperaccumulator was treated by the FJH treatment to synchronously achieve an efficient metal removal and material upgradation. (1) To evaluate the versatility of FJH treatment for hyperaccumulator recycling, reacting phenomena, metal removal efficiency, and the structure of derived materials were analyzed. (2) The crystal phase inducer was used to induce a pyrochlorination reaction to further improve the metal removal efficiency. (3) The seed germination assessment was conducted to analyze the environmental safety of the flash graphene. Finally, the superiority assessment of flash graphene was conducted to verify its wider applicability than pyrochar (PC). Also, the sample was treated by pyrolysis as comparison.

2. MATERIALS AND METHODS

2.1. Hyperaccumulator Recycling Using FJH. *Sedum plumbizincicola*, collected from a zinc (Zn) remediation site, was selected as a typical hyperaccumulator (mainly contains Zn). The FJH treatment was conducted in a homemade equipment, which included power, reacting, and product collecting system (Figures S2 and S3). The FJH equipment supplied an alternating current to directly graphitize and exfoliate the sample to promote metal volatilization and synchronously upgrade to flash graphene. *S. plumbizincicola* was first mixed with carbon black (6 wt %) to obtain a conductive sample. Further, KCl, as a typical crystal phase inducer, was added into this mixture to further improve metal removal. To initiate the FJH reaction, this mixture sample was treated by an alternating current at initial voltage from 80 to

https://doi.org/10.1021/acsestengg.3c00278
ACS EST Engg. 2023, 3, 1966−1974

200 V under a negative pressure. During the FJH treatment, volatiles flow through the hollow anode and were eventually trapped by collecting system. The collecting system consisted of a condenser pipe and a successional gas bag (Figures 1a, S2, and S4). The evaporated metals can be further condensed in the condenser pipe at the liquid N_2 temperature.

To take a closer observation at the synchronous action which included instantaneous metal evaporation, a high-speed camera (Qianyanlang M230) was applied to film the reacting process at 500 frames per second. Furthermore, the light intensity changes of the reacting sample were obtained from the video to investigate the graphitization process. Based on the Hue Saturation and Value color model, MATLAB software was used to extract light intensity of different positions along the horizontal center line of the reacting tube. Therefore, the light intensity distribution of the reacting area at an arbitrary time was obtained. Sequentially, the changes of light intensity with time in a fixed position of the reacting area were obtained by analyzing different screenshots of the video.

Moreover, the sample was treated by slow pyrolysis in comparison to the FJH treatment. The sample was pyrolyzed in a box-type resistance furnace with a continuous nitrogen gas flow of 100 mL/min at 600 °C (heating rate of 10 °C/min) for 90 min.

2.2. Assessment of the FJH-Derived Products. To assess the solid, liquid, and gaseous products of the FJH treatment, the products were, respectively, collected. FJH-derived carbon materials were named as FG80, FG140, and FG200 according to the initial voltage (80, 140, 200 V), and FG140-Cl represented the flash graphene produced under 140 V with the assistance of KCl crystal phase inducer. The FJH-derived carbon material was first digested to calculate metal removal efficiency (Note S1). Then, the Toxicity Characteristic Leaching Procedure and seed germination experiment were conducted to investigate the release risk of heavy metal (Zn), the details of which are listed in Note S1. Additionally, the intensity of environmental persistent radicals in the derived carbon samples was determined by an electron paramagnetic resonance (EPR) spectrometer (JEOL-FA200) with a single cavity. The parameters for the EPR measurement were as follows: the modulation was 100 kHz with the microwave frequencies of 9076 MHz, the sweep width was 100 G, and the modulation amplitude was 0.35 mT. The EPR microwave power was set specifically to 1 mW, and the sweep time was 81.92 ms. In order to identify the combined form of heavy metal (Zn) in carbon material, X-ray absorption spectra of the samples at Zn K-edge were collected. Zn foil and ZnO were used as reference standards. The storage ring was operated at the energy of 2.5 GeV with an average electron current below 200 mA. The $k2$-weighted Fourier transform of $x(k)$ in R space was obtained over a range of 0−14.0 Å by applying a base window. The acquired extended X-ray absorption fine structure (EXAFS) data were extracted and processed according to the standard procedures using the ATHENA module implemented in the FEFIT software packages.

Furthermore, the structure of the carbon material was assessed. Raman spectra were taken to identify the graphitization degree and the layer of the carbon material. The parameters were fitted with three distinctive Lorentz peaks: D (~1350 cm^{-1}), G (~1580 cm^{-1}), and 2D (~2700 cm^{-1}) bands. X-ray photoelectron spectroscopy (XPS) analysis was performed using a PHI Quantera XPS system using a step size of 0.1 eV with a pass energy of 26 eV. All of XPS spectra were calibrated using the standard C 1s peak at 284.8 eV. Atomic force microscopy (AFM) analysis was performed to measure the flake thickness of flash graphene by a Bruker AFM system (Bruker Dimension ICON, Germany). The details of other assessments (transmission electron microscope, surface area, and total pore volume analysis) are listed in Note S2.

As for the liquid products, the trapped samples were first concentrated by nitrogen blowing and dissolved in methyl alcohol for subsequent assessment. Chemical composition of liquid products was analyzed by electrospray ionization (ESI) Fourier transform (FT)-ICR MS (Bruker Apex ultra) in negative formation with a 15 T superconducting magnet. The capillary column-introduced voltage was 3.8 kV, and the accumulating time was 0.06 s. The signal-to-noise ratio was enhanced by accumulating 300 scans. Then, the statistics were analyzed to calculate the intensity weighted average values of O/C, H/C, DBE, and m/z for observing the transformation of the main chemical component of the samples.[24,25]

As for gaseous products, the samples were analyzed by gas chromatography (GC) (PerkinElmer Clarus 580) to identify the composition. The proportion and volume of small-molecule gases (such as H_2, CO, CO_2, C_2H_2, C_2H_4, C_2H_6, C_3H_6, and C_3H_8) were calculated to investigate the relationship between the FJH input power and the component changes.

The details of the superiority assessment for a high FJH power-derived flash graphene are listed in Notes S3 and S4.

3. RESULTS AND DISCUSSION

3.1. Hyperaccumulator Recycling Using FJH. *S. plumbizincicola*, a typical hyperaccumulator mainly containing Zn, was selected to disclose and examine the advantages of FJH treatment on hyperaccumulator recycling using a homemade equipment (Figures 1a, S2, and S3 and Table S1). Based on the changes in current, temperature, and phenomena visualized using a high-speed camera (Figures S5 and S6), the FJH treatment with an initial voltage of 140 V could be typically divided into three stages (Figure 1b). In the initial stage (0−0.6 s), the alternating current induced Joule heat that instantaneously heated the sample to increase its temperature with an ~90% reduction in sample resistance (Figures 1c and S7 and Table S2). Next (0.6−2 s), the decrease in the sample resistance will lead to the increase in the current (Figure 1b). Undoubtedly, the temperature can rapidly increase over most metal boiling points due to the stronger heating effect caused by the increasing current (Figure 1b), implying a possible high metal removal efficiency. Accordingly, a few luminous spots and smoke were discharged from the reacting tube with a bright pink light emitted from the sample (Figures 1d and S8). The pink light exhibited a mixed color from ionized metals (endogenous Ca and Mg in the hyperaccumulator), implying that the temperature was high enough to evaporate endogenous metals (Figure 1e). It also should be noted that the evaporated metals can be trapped by the collecting system with liquid N_2 of the FJH equipment (Figure S4). Subsequently (2−20 s), the sample was heated to incandescence with a rapid change of temperature from 1400 to 3000 K and graphitized under ultrahigh temperature in the remolding stage (Figure 1f). During the remolding stage, the light intensity of the sample rapidly increased, and the luminous area extended to the whole sample, indicating the thorough graphitization of the sample (Figures 1g and S9). Additionally, the strong current repeatedly shocked the

https://doi.org/10.1021/acsestengg.3c00278
ACS EST Engg. 2023, 3, 1966−1974

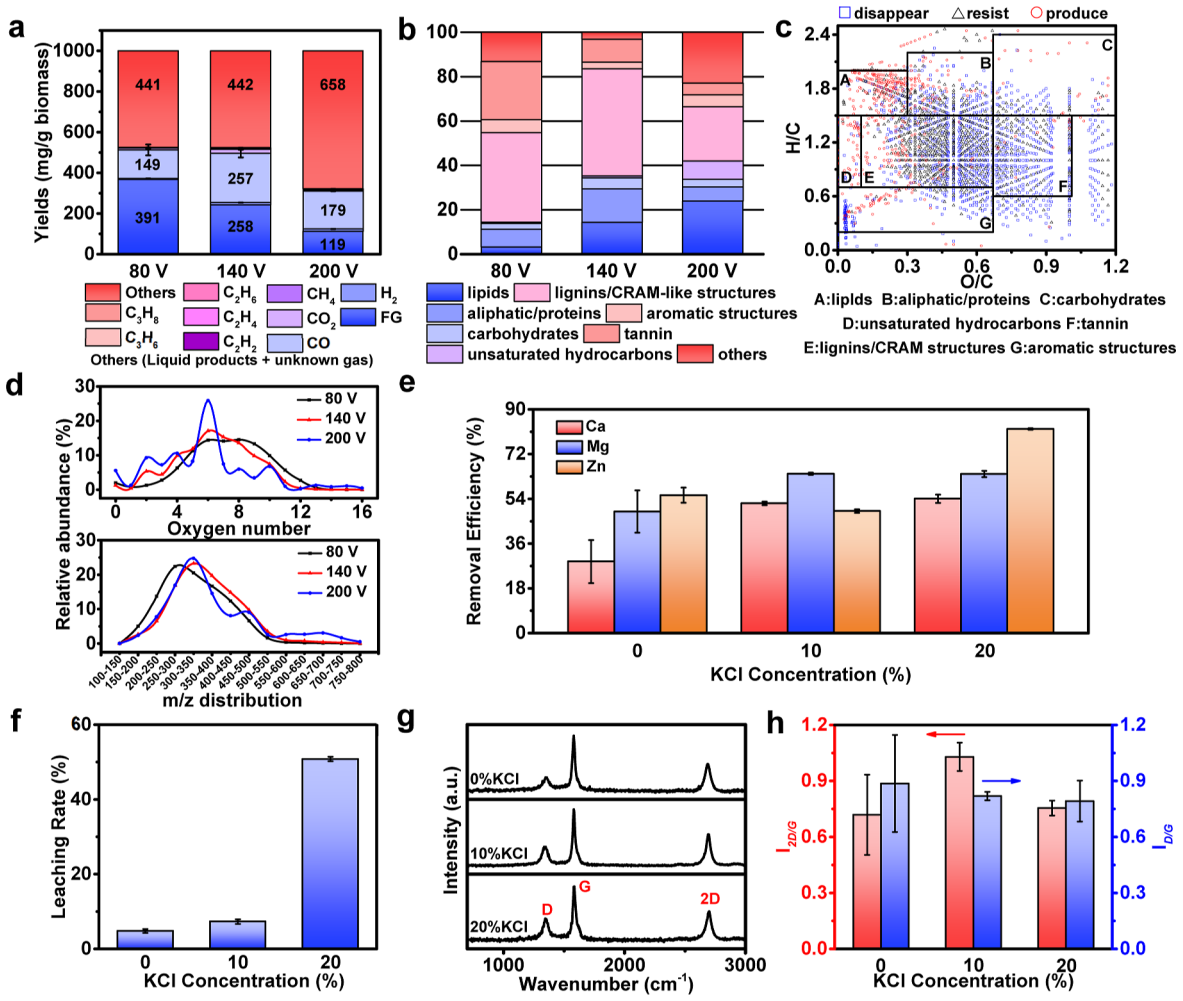

Figure 2. (a) Mass distribution of solid, liquid, and gaseous products of the FJH treatment. (b) Chemical composition (%) of liquid products of the FJH treatment with different initial voltages. (c) Plots of O/C versus H/C for the resistant, produced, and reacted compounds of the FJH treatment with the initial voltage of 200 V compared with 80 V. (d) O_x class species and m/z distribution of the liquid products of the FJH treatment with different initial voltages. (e) Metal removal efficiency of the FJH treatment with different concentrations of KCl. (f) Zn leaching rate of various flash graphene derived from the FJH treatment with different concentrations of KCl. (g) Raman spectra of various flash graphene derived from the FJH treatment with different concentrations of KCl. (h) $I_{2D/G}$ and $I_{D/G}$ ratios of various flash graphene derived from the FJH treatment with different concentrations of KCl. The error bars represent the standard deviation where each sample was tested for 2 times.

graphitized sample to exfoliate the carbon layer. Thus, this unique process, which included an instantaneous high temperature and a strong current, could lead to synchronous metal evaporation, graphitization, and exfoliation of the sample.

As predicted, the FJH treatment achieved a higher metal removal efficiency than that of pyrolysis recycling (Figures 1h and S10). Furthermore, the metal removal efficiency of the FJH treatment improved with the increase of input power due to the enhanced reacting temperature (Figures S11−S13 and Note S5). Importantly, as a risky heavy metal that may induce secondary pollution, the leaching risk of Zn from the FJH-derived carbon material was lower than that of the international Zn leaching standard (Figure S14). This was because the concentration of the remaining Zn in the FJH-derived carbon material was low and the combined form of Zn became more stable after treatment with an ultrahigh temperature. In addition, the reduced $I_{D/G}$ value and the increased $I_{2D/G}$ value indicated that the sample was graphitized and exfoliated to a thin flash graphene at a high input power (Figures 1i and S15). The thickness of the material produced under a high initial voltage (FG140 represents the FJH-derived carbon material under a voltage of 140 V) was observed to be 0.90−2.34 nm (Figure S16), indicating that the stronger power promoted the graphitization of the carbon material and reinforced electric exfoliation to produce a flash graphene structure with a few layers, which was also confirmed by the transmission electron microscopy image of FG140. XPS analysis indicated a high ratio of C═C to C−C bonds with an increase in the input power, further confirming the formation of a flash graphene structure at high input power (Figure S17 and Table S3).[17]

To evaluate the advantages of FJH treatment, the sample was also treated with pyrolysis for comparison. In addition to the low metal removal efficiency, pyrolysis produced low-quality PC with an inferior carbon structure due to the low reacting temperature and the lack of electric exfoliating effect (Figures 1i and S18). Additionally, PC also had a high Zn leaching risk because of the high Zn concentration and the unstable combined state (Figures S14 and S19). There were no differences in the pore structures of PC and flash graphene (Figure S20 and Table S4). Therefore, the FJH treatment

https://doi.org/10.1021/acsestengg.3c00278
ACS EST Engg. 2023, 3, 1966−1974

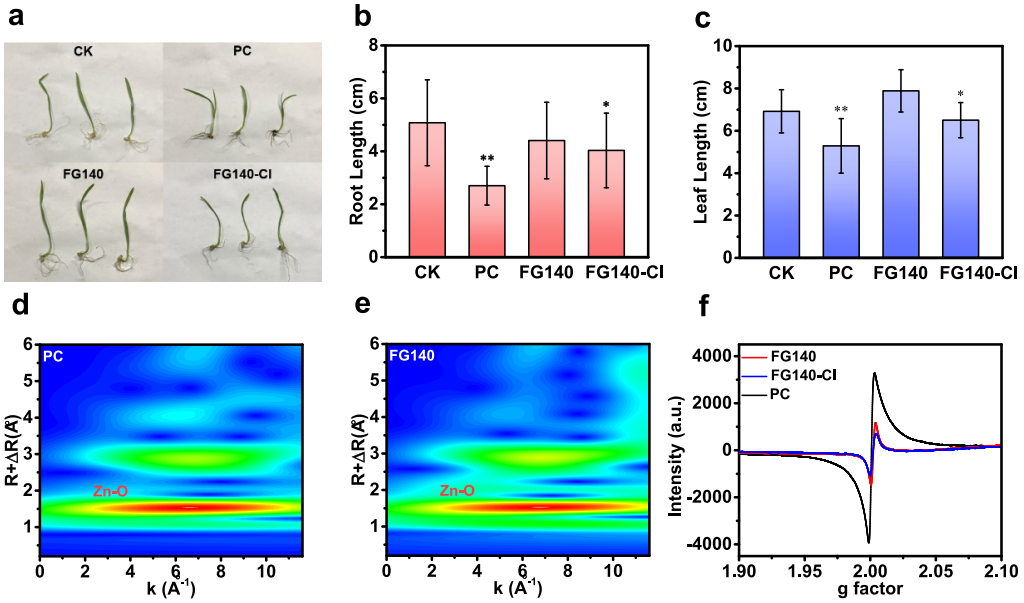

Figure 3. (a) Comparison of wheat seed growth treated by different solutions (1% w/w) after 7 days. CK corresponds to the control sample. (b,c) Effects of different samples on the length of root and shoot of the wheat seedling. (* and ** represent statistically significant at $p < 0.05$ and $p < 0.01$ compared to control). (d,e) Wavelet transform images of PC and flash graphene. The red area represents the combined bond of Zn. (f) Free radical signal of various samples. g factor indicates the form of free radicals.

conquered obstacles inherent in traditional techniques, showing a superior ability for synchronous graphene fabrication and metal removal.

Additionally, the liquid and gaseous products of the FJH treatment, which accounted for 60.9−88.1% weight, were also investigated (Figure 2a). GC and high-resolution FT-ICR MS with negative ESI were used to reveal how liquid and gaseous products transformed under different input powers. With increased input power, compounds with high H/C values but low O/C values were produced (Table S5), indicating that FJH induced a decarboxylation reaction based on the van Krevelen diagram (Figure S21). Moreover, the molecular composition indicated that the main contents (tannin, lignin, and carboxylic-rich alicyclic molecule (CRAM)-like structures) of the liquid products were further degraded to lipids with increased input power (Figures 2b,c and S22), which was consistent with the increased H/C values and the reduced O/C values. Accordingly, highly oxidized compounds were cracked and transformed to gaseous products (Figures 2d and S23). Since the gaseous products mainly consisted of available CO, H_2, and CH_4 (Figure S24), they might be utilized for power generation to offset the partial energy of the FJH treatment.

3.2. Decontamination Improvement with the Assistance of Crystal Phase Inducer. Pyrochlorination refining has been used to improve the metal recovery efficiency of pyrometallurgy.[26,27] Therefore, KCl was added to the reactant as a crystal phase inducer to improve the metal removal efficiency during the FJH treatment. With the addition of the crystal phase inducer, metal removal efficiency was promoted (Figure 2e) because the crystal phase inducer converted the inherent metal into metal chloride. Since metal chloride has a higher vapor pressure than metal, inherent metals were evaporated better when the sample was electrified (Figure S25). Notably, Zn removal efficiency promoted from 55.5 to 82.1%. Accordingly, the Zn enrichment factor significantly decreased to 0.83 (Figure S26), indicating that the absolute Zn concentration in flash graphene was lower than that in the raw material. Therefore, the crystal phase inducer improved the decontamination ability of the FJH treatment. Additionally, over 50.8% of Zn that remained in the produced flash graphene could be leached out (Figure 2f), indicating that the flash graphene could be further purified with a second leaching process using harmless solution. After secondary leaching, the Zn removal efficiency of FJH treatment was enhanced to 98.6% (Figure S27).

Next, the influence of the crystal phase inducer on the graphene fabrication ability of the FJH treatment was investigated. There were no significant differences in the temperature and current of the FJH treatment (Figure S28), implying that the carbon structure rearrangement might not be hindered by the crystal phase inducer. As predicted, Raman spectra of the produced flash graphene showed an apparent 2D band, confirming that the addition of the crystal phase inducer did not suppress the graphitization and electric exfoliation of the sample (Figure 2g,h). Therefore, the crystal phase inducer can optimize the decontamination capacity of the FJH treatment under less negative impacts on graphene fabrication ability.

3.3. Environmental Safety of Flash Graphene Produced Using FJH Treatment. The FJH treatment with a high initial voltage exhibited a high metal removal efficiency and improvement in the structure of the derived carbon materials. Therefore, FG140, FG140-Cl, and PC (FG140-Cl represents flash graphene produced under 140 V with the assistance of the KCl crystal phase inducer) were chosen to conduct an environmental assessment using seed germination.[28−30] Flash graphene exhibited little negative impact on wheat growth (Figure 3a), whereas PC obviously inhibited the growth of wheat (Figure 3b,c). It was reported that heavy metals might hinder plant growth,[31,32] implying that higher Zn leaching risk of PC leads to inhibition of plant growth. FT EXAFS spectra of both flash graphene and PC showed that the bond length of the first Zn core was ~2 Å (Figure S29),

https://doi.org/10.1021/acsestengg.3c00278
ACS EST Engg. 2023, 3, 1966−1974

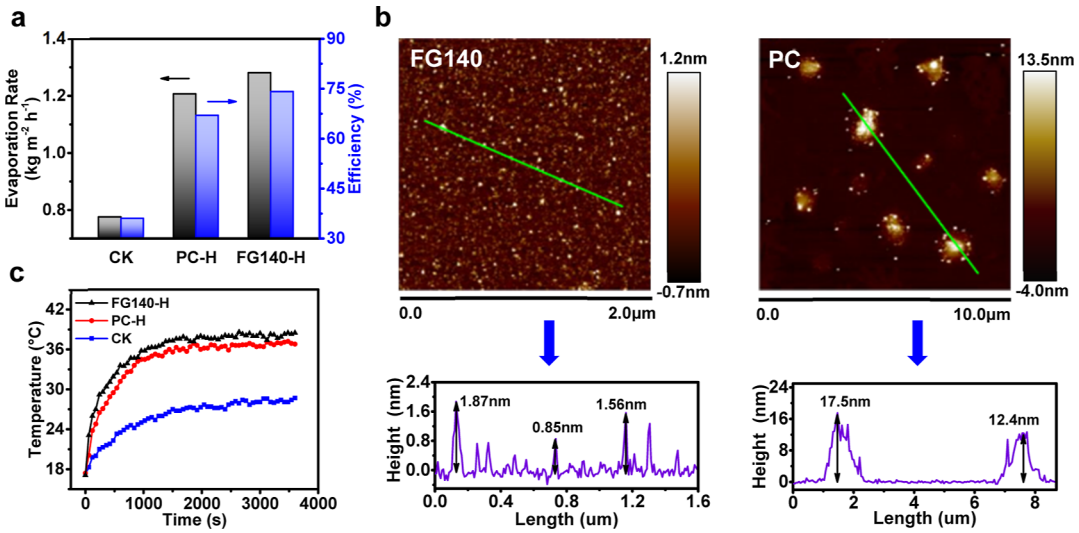

Figure 4. (a) Evaporation rate and evaporation efficiency of different hydrogels under 1 sun irradiation. (FG140-H represents flash graphene FG140-derived hybrid hydrogel, PC-H represents PC-derived hybrid hydrogel, and CK represents pure hydrogel.) (b) AFM analysis of flash graphene and PC. The below plots represent the thickness and morphology of the selected parts of the above plots. (c) Temperature changes of each hydrogel surface under 1 sun irradiation.

indicating that zinc oxide was the main compound remaining in the samples. Additionally, the wavelet transform spectra of both samples confirmed that the main combined form of Zn did not change under higher temperatures (Figures 3d,e and S30). According to the EXAFS fitting parameters of flash graphene and PC, the coordination number of Zn was slightly larger in flash graphene (Figure S31 and Table S6), indicating that ZnO was more stable after the FJH treatment. Accordingly, the Zn leaching concentration in FG140 was lower than that in PC, which partly accounted for little growth inhibition of wheat seeds treated with FG140.

In addition, environmentally persistent free radicals (EPFRs) in the samples may synchronously cause negative impacts on seed growth by inducing $^{\bullet}$OH in water.[33−36] An EPFR signal was detected in both flash graphene and PC (Figure 3f). Since all g factors of the EPFR signals ranged from 2 to 2.003 (Table S7), the EPFRs of all samples were carbon-centered radicals.[37] Further, high temperature (>1173 K) is able to promote EPFR decomposition.[38] As shown in Figure 3f, the EPFR intensity in flash graphene is ∼3 times lower than that in PC, suggesting that flash graphene contains less EPFRs. Accordingly, low concentration of EPFRs induced less $^{\bullet}$OH in water,[39,40] imposing little inhibition on seed growth compared to that of PC. Therefore, both the low heavy metal concentration and fewer EPFRs in flash graphene had fewer impacts on wheat seed growth, indicating that flash graphene was relatively environmentally safe.

3.4. Superiority Assessment of Flash Graphene Derived from FJH Treatment. As a promising two-dimensional material, graphene has revolutionized a wide range of applications.[41,42] Thus, flash graphene was used as a specimen to assess its superiority over PC by photothermal conversion. Flash graphene was used to fabric a hybrid hydrogel (FG140-H) as a solar evaporator in comparison with a pure hydrogel (CK) and a PC-derived hybrid hydrogel (PC-H) for solar-driven water evaporation under 1 sun irradiation.[43] As shown in Figure 4a, FG140-H has a better performance with an energy conversion efficiency of 74.1% compared with that of CK (36.0%) and PC-H (67.0%). As shown in Figures 4b and S32, flash graphene has a smaller particle size (20−40 nm) and reduced thickness (0.85−1.87 nm) compared to that of PC, which results in better interpenetration of flash graphene in the polymeric network of the hydrogel to enhance heat confinement and accelerate water evaporation.[44,45] Therefore, the surface temperature of FG140-H was higher and increased faster than that of PC-H (Figures 4c and S33), resulting in increased water evaporation efficiency of FG140-H. Moreover, flash graphene with a thin layer showed high thermal conductivity due to faster electron transfer, which enabled FG140-H to fast transfer thermal energy into the surrounding polymeric network to improve evaporation.[46,47] Additionally, broadband light absorption also improves the efficiency of solar-driven water evaporation.[48−51] As shown in Figure S34, FG140-H and PC-H show similar light absorption (92.0−96.1%) over a broad solar spectrum (250−2500 nm) because dark materials show similar light absorption ability. Therefore, it can be deduced that the small particle size and a thin layer enabled flash graphene to achieve a better water evaporation efficiency.

Next, the comprehensive ability of FG140-H was assessed. Hydrophilicity has a significant influence on the water content, which affects the water evaporation process.[52] The contact angle of the surface of FG140-H was 47.59° (Figure S35), which illustrated that FG140-H was hydrophilic enough to absorb bulk water. As shown in Figure S36, the saturated water content of FG140-H is 5.0 g/g, which ensures a sufficient water supply to achieve a high water evaporation efficiency. Further, small pores were detected in FG140-H, and the pore walls also contained small pores (Figure S37). The rich pore structure enabled FG140-H to supply sufficient water to the hydrogel surface. Therefore, the FJH-derived graphene showed superior application potential than PC.

Overall, the FJH treatment achieved an efficient metal removal and synchronously upgraded a hazardous hyper-accumulator to a profitable material (flash graphene), which cannot be achieved by the traditional pyrolysis treatment.

https://doi.org/10.1021/acsestengg.3c00278
ACS EST Engg. 2023, 3, 1966−1974

4. CONCLUSIONS

In this work, the hazardous hyperaccumulator is recycled using an innovative FJH treatment to gain a more profitable material (flash graphene) with a few remaining metals. Compared to the traditional pyrolysis treatment, the FJH treatment proves to be a win−win method for decontamination and value increment of hyperaccumulator. With the assistance of a crystal phase inducer, the decontamination capacity of the FJH treatment was optimized under less negative impacts on the graphene fabrication ability. Also, the FJH-derived flash graphene, with a few remaining metals or environmentally persistent radicals, was shown to be environmentally safe. Moreover, the hybrid hydrogel manufactured with flash graphene showed better performance on photothermal conversion for solar-driven water evaporation. An economic evaluation of the FJH treatment and the pyrolysis treatment (Note S5 and Table S8) indicated that the FJH treatment showed a net income of ∼850 times that of the profits of pyrolysis. Therefore, a considerable value increment of the FJH treatment can be achieved by construction of an amplifying automatic FJH system to further promote the manufacturing capacity.[17]

■ ASSOCIATED CONTENT

Supporting Information

The Supporting Information is available free of charge at https://pubs.acs.org/doi/10.1021/acsestengg.3c00278.

Schematic of homemade FJH equipment; phenomena of the FJH treatment visualized using a high-speed camera; real-time voltage, current, and temperature during the FJH treatment; TEM, atomic force microscopy analysis, and other characterization graphs of flash graphene and PC; van Krevelen diagrams of liquid products of the FJH treatment; and economic analysis of the FJH treatment and the traditional pyrolysis treatment (PDF)

■ AUTHOR INFORMATION

Corresponding Author

Xiangdong Zhu − *Department of Environmental Science and Engineering, Fudan University, Shanghai 200438, China;* orcid.org/0000-0002-8536-7690; Email: zxdjewett@fudan.edu.cn

Authors

Zhelin He − *Department of Environmental Science and Engineering, Fudan University, Shanghai 200438, China*

Chao Jia − *Department of Environmental Science and Engineering, Fudan University, Shanghai 200438, China*

Long Cheng − *School of Energy and Power Engineering, Jiangsu University of Science and Technology, Zhenjiang, Jiangsu 212100, China*

Fengbo Yu − *Department of Environmental Science and Engineering, Fudan University, Shanghai 200438, China*

Liming Sun − *Department of Environmental Science and Engineering, Fudan University, Shanghai 200438, China*

Litao Lin − *Department of Environmental Science and Engineering, Fudan University, Shanghai 200438, China*

Tao Teng − *Department of Environmental Science and Engineering, Fudan University, Shanghai 200438, China*

Xuan Wu − *Department of Environmental Science and Engineering, Fudan University, Shanghai 200438, China*

Jie Gao − *Department of Environmental Science and Engineering, Fudan University, Shanghai 200438, China*

Linzhi Zuo − *School of Energy and Power Engineering, Jiangsu University of Science and Technology, Zhenjiang, Jiangsu 212100, China*

Ting Bian − *School of Energy and Power Engineering, Jiangsu University of Science and Technology, Zhenjiang, Jiangsu 212100, China*

Liang Wang − *School of Energy and Power Engineering, Jiangsu University of Science and Technology, Zhenjiang, Jiangsu 212100, China*

Shicheng Zhang − *Department of Environmental Science and Engineering, Fudan University, Shanghai 200438, China;* orcid.org/0000-0001-9994-1385

Complete contact information is available at: https://pubs.acs.org/10.1021/acsestengg.3c00278

Author Contributions

Z. L. He, C. Jia, and X. D. Zhu conceived the idea to use FJH to remove heavy metals in a hazardous hyperaccumulator synchronizing with the fabrication of flash graphene. Z. L. He, C. Jia, and L. Cheng conducted most of the experimental work with the help of F. B. Yu, L. M. Sun, L. T. Lin, T. Teng, X. Wu, J. Gao, L. Z. Zuo, T. Bian, L. Wang, and S. C. Zhang. All aspects of the research were overseen by X. D. Zhu. All authors discussed the results and commented on the manuscript. CRediT: **Zhelin He** investigation, methodology; **Chao Jia** investigation; **Long Cheng** investigation; **Fengbo Yu** investigation; **Liming Sun** investigation; **Litao Lin** investigation; **Tao Teng** investigation; **Xuan Wu** investigation; **Jie Gao** investigation; **Linzhi Zuo** investigation; **Ting Bian** investigation; **Liang Wang** investigation; **Shicheng Zhang** investigation; **Xiangdong Zhu** investigation, methodology.

Notes

The authors declare no competing financial interest.

■ ACKNOWLEDGMENTS

This research was supported by fund from the National Natural Science Foundation of China (grant no. 22276040).

■ REFERENCES

(1) Jin, Y.; Wang, L.; Song, Y.; Zhu, J.; Qin, M.; Wu, L.; Hu, P.; Li, F.; Fang, L.; Chen, C.; Hou, D. Integrated life cycle assessment for sustainable remediation of contaminated agricultural soil in China. *Environ. Sci. Technol.* **2021**, *55*, 12032−12042.

(2) Li, J. T.; Gurajala, H. K.; Wu, L. H.; van der Ent, A.; Qiu, R. L.; Baker, A. J. M.; Tang, Y. T.; Yang, X. E.; Shu, W. S. Hyperaccumulator plants from china: A synthesis of the current state of knowledge. *Environ. Sci. Technol.* **2018**, *52*, 11980−11994.

(3) Han, R.; Chen, J. Y.; He, S. X.; Liu, C. J.; Dai, Z. H.; Liu, X.; Cao, Y.; Ma, L. Q. Phytate and arsenic enhance each other's uptake in as-hyperaccumulator Pteris vittata: Root exudation of phytate and phytase, and plant uptake of phytate-P. *Environ. Sci. Technol.* **2023**, *57*, 190−200.

(4) Smoak, R. A.; Schnoor, J. L. Nickel hyperaccumulator biochar as a ni-adsorbent and enhanced bio-ore. *ACS Environ. Au* **2022**, *2*, 65−73.

(5) Yang, Q.; Wang, W.; Zhou, Y.; Hao, J.; Fang, G.; Liu, C.; Cui, P.; Wang, Y. Facile pyrolysis treatment for the synthesis of single-atom mn catalysts derived from a hyperaccumulator. *ACS ES&T Engg* **2023**, *3*, 616−626.

(6) Cui, X.; Zhang, J.; Wang, X.; Pan, M.; Lin, Q.; Khan, K. Y.; Yan, B.; Li, T.; He, Z.; Yang, X.; Chen, G. A review on the thermal

treatment of heavy metal hyperaccumulator: Fates of heavy metals and generation of products. *J. Hazard. Mater.* **2021**, *405*, 123832.
(7) Kiciński, W.; Dyjak, S. Transition metal impurities in carbon-based materials: Pitfalls, artifacts and deleterious effects. *Carbon* **2020**, *168*, 748−845.
(8) Yuan, Z.; Huang, Q.; Wang, Z.; Wang, H.; Luo, J.; Zhu, N.; Cao, X.; Lou, Z. Medium-low temperature conditions induce the formation of environmentally persistent free radicals in microplastics with conjugated aromatic-ring structures during sewage sludge pyrolysis. *Environ. Sci. Technol.* **2022**, *56*, 16209−16220.
(9) Xiang, L.; Harindintwali, J. D.; Wang, F.; Redmile-Gordon, M.; Chang, S. X.; Fu, Y.; He, C.; Muhoza, B.; Brahushi, F.; Bolan, N.; Jiang, X.; Ok, Y. S.; Rinklebe, J.; Schaeffer, A.; Zhu, Y. G.; Tiedje, J. M.; Xing, B. Integrating biochar, bacteria, and plants for sustainable remediation of soils contaminated with organic pollutants. *Environ. Sci. Technol.* **2022**, *56*, 16546−16566.
(10) Wang, J.; Xu, Z. Disposing and recycling waste printed circuit boards: Disconnecting, resource recovery, and pollution control. *Environ. Sci. Technol.* **2015**, *49*, 721−733.
(11) Du, J.; Zhang, L.; Liu, T.; Xiao, R.; Li, R.; Guo, D.; Qiu, L.; Yang, X.; Zhang, Z. Thermal conversion of a promising phytoremediation plant (symphytum officinale l.) into biochar: Dynamic of potentially toxic elements and environmental acceptability assessment of the biochar. *Bioresour. Technol.* **2019**, *274*, 73−82.
(12) Chai, Y.; Bai, M.; Chen, A.; Peng, L.; Shao, J.; Shang, C.; Peng, C.; Zhang, J.; Zhou, Y. Thermochemical conversion of heavy metal contaminated biomass: Fate of the metals and their impact on products. *Sci. Total Environ.* **2022**, *822*, 153426.
(13) Lu, S.; Du, Y.; Zhong, D.; Zhao, B.; Li, X.; Xu, M.; Li, Z.; Luo, Y.; Yan, J.; Wu, L. Comparison of trace element emissions from thermal treatments of heavy metal hyperaccumulators. *Environ. Sci. Technol.* **2012**, *46*, 5025−5031.
(14) Wu, P.; Wang, Z.; Wang, H.; Bolan, N. S.; Wang, Y.; Chen, W. Visualizing the emerging trends of biochar research and applications in 2019: A scientometric analysis and review. *Biochar* **2020**, *2*, 135−150.
(15) Shi, S.; Jia, C.; Huo, X.; Zhang, S.; Xu, Q.; Zhu, X. Thermal stabilization effect and oxygen replacement reaction together regulate n/s co-doped microporous carbon synthesis. *Carbon Res.* **2022**, *1*, 7.
(16) Jia, C.; Pang, M.; Lu, Y.; Liu, Y.; Zhuang, M.; Liu, B.; Lu, J.; Wei, T.; Wang, L.; Bian, T.; Wang, M.; Yu, F.; Sun, L.; Lin, L.; Teng, T.; Wu, X.; He, Z.; Gao, J.; Luo, J.; Zhang, S.; Feng, L.; Yin, X.; You, F.; Li, G.; Zhang, L.; Zhu, Y.-G.; Zhu, X.; Yang, Y. Graphene environmental footprint greatly reduced when derived from biomass waste via flash joule heating. *One Earth* **2022**, *5*, 1394−1403.
(17) Luong, D. X.; Bets, K. V.; Algozeeb, W. A.; Stanford, M. G.; Kittrell, C.; Chen, W.; Salvatierra, R. V.; Ren, M.; McHugh, E. A.; Advincula, P. A.; Wang, Z.; Bhatt, M.; Guo, H.; Mancevski, V.; Shahsavari, R.; Yakobson, B. I.; Tour, J. M. Gram-scale bottom-up flash graphene synthesis. *Nature* **2020**, *577*, 647−651.
(18) Cheng, Y.; Cheng, S.; Chen, B.; Jiang, J.; Tu, C.; Li, W.; Yang, Y.; Huang, K.; Wang, K.; Yuan, H.; Li, J.; Qi, Y.; Liu, Z. Graphene infrared radiation management targeting photothermal conversion for electric-energy-free crude oil collection. *J. Am. Chem. Soc.* **2022**, *144*, 15562−15568.
(19) Cheng, Y.; Cui, G.; Liu, C.; Liu, Z.; Yan, L.; Liu, B.; Yuan, H.; Shi, P.; Jiang, J.; Huang, K.; Wang, K.; Cheng, S.; Li, J.; Gao, P.; Zhang, X.; Qi, Y.; Liu, Z. Electric current aligning component units during graphene fiber joule heating. *Adv. Funct. Mater.* **2021**, *32*, 210349.
(20) Chen, W.; Ge, C.; Li, J. T.; Beckham, J. L.; Yuan, Z.; Wyss, K. M.; Advincula, P. A.; Eddy, L.; Kittrell, C.; Chen, J.; Luong, D. X.; Carter, R. A.; Tour, J. M. Heteroatom-doped flash graphene. *ACS Nano* **2022**, *16*, 6646−6656.
(21) Deng, B.; Meng, W.; Advincula, P. A.; Eddy, L.; Ucak-Astarlioglu, M. G.; Wyss, K. M.; Chen, W.; Carter, R. A.; Li, G.; Cheng, Y.; Nagarajaiah, S.; Tour, J. M. Heavy metal removal from coal fly ash for low carbon footprint cement. *Chem. Eng.* **2023**, *2*, 13.
(22) Algozeeb, W. A.; Savas, P. E.; Luong, D. X.; Chen, W.; Kittrell, C.; Bhat, M.; Shahsavari, R.; Tour, J. M. Flash graphene from plastic waste. *ACS Nano* **2020**, *14*, 15595−15604.
(23) Deng, B.; Luong, D. X.; Wang, Z.; Kittrell, C.; McHugh, E. A.; Tour, J. M. Urban mining by flash joule heating. *Nat. Commun.* **2021**, *12*, 5794.
(24) Shang, H.; Zhang, S.; Zhu, X. Biomass cellulose component and fe mineral catalysis help Cr(vi) to realize almost 100% pyrolysis reduction efficiency. *ACS ES&T Engg* **2021**, *1*, 1441−1448.
(25) Yu, F.; Zhao, W.; Qin, T.; Zhao, W.; Chen, Y.; Miao, X.; Lin, L.; Shang, H.; Sui, G.; Peng, D.; Yang, Y.; Zhu, Y.; Zhang, S.; Zhu, X. Biosafety of human environments can be supported by effective use of renewable biomass. *Proc. Natl. Acad. Sci. U.S.A.* **2022**, *119*, No. e2106843119D.
(26) Chen, Y.; Shang, H. J.; Ren, Y. Q.; Yue, Y. H.; Li, H. X.; Bian, Z. F. Systematic assessment of precious metal recovery to improve environmental and resource protection. *ACS ES&T Engg* **2022**, *2*, 1039−1052.
(27) Cui, X.; Zhang, J.; Pan, M.; Lin, Q.; Khan, M. B.; Yang, X.; He, Z.; Yan, B.; Chen, G. Double-edged effects of polyvinyl chloride addition on heavy metal separation and biochar production during pyrolysis of Cd/Zn hyperaccumulator. *J. Hazard. Mater.* **2021**, *416*, 125793.
(28) Luo, J.; Wang, Q.; Lin, L.; Zhang, S.; Zhu, X. Waste plastics complement biochar: Innovative approach in curbing toxicants (KCN/NaCN) in n-containing biochar. *ACS Sustain. Chem. Eng.* **2021**, *9*, 4617−4624.
(29) Zhang, K.; Wang, Y.; Mao, J.; Chen, B. Effects of biochar nanoparticles on seed germination and seedling growth. *Environ. Pollut.* **2020**, *256*, 113409.
(30) Singh, M.; Ahsan, M.; Pandey, V.; Singh, A.; Mishra, D.; Tiwari, N.; Singh, P.; Karak, T.; Khare, P. Comparative assessment for removal of anionic dye from water by different waste-derived biochar vis a vis reusability of generated sludge. *Biochar* **2022**, *4*, 13.
(31) Prechthai, T.; Parkpian, P.; Visvanathan, C. Assessment of heavy metal contamination and its mobilization from municipal solid waste open dumping site. *J. Hazard. Mater.* **2008**, *156*, 86−94.
(32) Huang, G. Y.; Wang, Y. S. Physiological and biochemical responses in the leaves of two mangrove plant seedlings (kandelia candel and bruguiera gymnorrhiza) exposed to multiple heavy metals. *J. Hazard. Mater.* **2010**, *182*, 848−854.
(33) Zhao, Z.; Chen, Q.; Li, H.; Lang, D.; Wu, M.; Zhou, D.; Pan, B.; Xing, B. The exposed hematite surface and the generation of environmentally persistent free radicals during catechol degradation. *Environ. Sci.: Processes Impacts* **2021**, *23*, 109−116.
(34) Zhao, L.; Liang, N.; Lang, D.; Zhou, D.; Dong, X.; Peng, J.; Liu, L.; Pan, B.; Xing, B. Heating methods generate different amounts of persistent free radicals from unsaturated fatty acids. *Sci. Total Environ.* **2019**, *672*, 16−22.
(35) Lieke, T.; Zhang, X.; Steinberg, C. E. W.; Pan, B. Overlooked risks of biochars: Persistent free radicals trigger neurotoxicity in caenorhabditis elegans. *Environ. Sci. Technol.* **2018**, *52*, 7981−7987.
(36) Duan, W.; Oleszczuk, P.; Pan, B.; Xing, B. Environmental behavior of engineered biochars and their aging processes in soil. *Biochar* **2019**, *1*, 339−351.
(37) Tao, W.; Yang, X.; Li, Y.; Zhu, R.; Si, X.; Pan, B.; Xing, B. Components and persistent free radicals in the volatiles during pyrolysis of lignocellulose biomass. *Environ. Sci. Technol.* **2020**, *54*, 13274−13281.
(38) Wang, Y.; Yang, Q.; Chen, J.; Yang, J.; Zhang, Y.; Chen, Y.; Li, X.; Du, W.; Liang, A.; Ho, S. H.; Chang, J. S. Adsorption behavior of Cr(vi) by magnetically modified enteromorpha prolifera based biochar and the toxicity analysis. *J. Hazard. Mater.* **2020**, *395*, 122658.
(39) Liao, S.; Pan, B.; Li, H.; Zhang, D.; Xing, B. Detecting free radicals in biochars and determining their ability to inhibit the germination and growth of corn, wheat and rice seedlings. *Environ. Sci. Technol.* **2014**, *48*, 8581−8587.

https://doi.org/10.1021/acsestengg.3c00278
ACS EST Engg. 2023, 3, 1966−1974

(40) Vejerano, E. P.; Rao, G.; Khachatryan, L.; Cormier, S. A.; Lomnicki, S. Environmentally persistent free radicals: Insights on a new class of pollutants. *Environ. Sci. Technol.* **2018**, *52*, 2468−2481.
(41) Dong, S.; Xu, Y.; Wang, C.; Liu, C.; Zhang, J.; Di, Y.; Yu, L.; Dong, L.; Gan, Z. Atmospheric water harvester-assisted solar steam generation for highly efficient collection of distilled water. *J. Mater. Chem. A* **2022**, *10*, 1885−1890.
(42) Lu, D.; Zhou, Z.; Wang, Z.; Ho, D. T.; Sheng, G.; Chen, L.; Zhao, Y.; Li, X.; Cao, L.; Schwingenschlogl, U.; Ma, J.; Lai, Z. An ultrahigh-flux nanoporous graphene membrane for sustainable seawater desalination using low-grade heat. *Adv. Mater.* **2022**, *34*, No. e2109718.
(43) Chen, X.; He, S.; Falinski, M. M.; Wang, Y.; Li, T.; Zheng, S.; Sun, D.; Dai, J.; Bian, Y.; Zhu, X.; Jiang, J.; Hu, L.; Ren, Z. J. Sustainable off-grid desalination of hypersaline waters using janus wood evaporators. *Energy Environ. Sci.* **2021**, *14*, 5347−5357.
(44) Wang, Z.; Thomas, H.; Anthony, P.; Ngai, Y.; Li, D.; Elimelech, M.; Lin, S. Pathways and challenges for efficient solar-thermal desalination. *Sci. Adv.* **2019**, *5*, No. eaax0763.
(45) Zhou, X. Y.; Zhao, F.; Guo, Y. H.; Zhang, Y.; Yu, G. H. A hydrogel-based antifouling solar evaporator for highly efficient water desalination. *Energy Environ. Sci.* **2018**, *11*, 1985−1992.
(46) Wang, Y.; Wu, X.; Wu, P.; Zhao, J.; Yang, X.; Owens, G.; Xu, H. Enhancing solar steam generation using a highly thermally conductive evaporator support. *Sci. Bull.* **2021**, *66*, 2479−2488.
(47) Zhang, C.; Liang, H. Q.; Xu, Z. K.; Wang, Z. Harnessing solar-driven photothermal effect toward the water-energy nexus. *Adv. Sci.* **2019**, *6*, 1900883.
(48) Zhou, X.; Guo, Y.; Zhao, F.; Yu, G. Hydrogels as an emerging material platform for solar water purification. *Acc. Chem. Res.* **2019**, *52*, 3244−3253.
(49) Ren, H.; Tang, M.; Guan, B.; Wang, K.; Yang, J.; Wang, F.; Wang, M.; Shan, J.; Chen, Z.; Wei, D.; Peng, H.; Liu, Z. Hierarchical graphene foam for efficient omnidirectional solar-thermal energy conversion. *Adv. Mater.* **2017**, *29*, 1702590.
(50) Li, Y.; Gao, T.; Yang, Z.; Chen, C.; Luo, W.; Song, J.; Hitz, E.; Jia, C.; Zhou, Y.; Liu, B.; Yang, B.; Hu, L. 3D-printed, all-in-one evaporator for high-efficiency solar steam generation under 1 sun illumination. *Adv. Mater.* **2017**, *29*, 1700981.
(51) Zhang, Y.; Xiong, T.; Nandakumar, D. K.; Tan, S. C. Structure architecting for salt-rejecting solar interfacial desalination to achieve high-performance evaporation with in situ energy generation. *Adv. Sci.* **2020**, *7*, 1903478.
(52) Li, C.; Cao, S.; Lutzki, J.; Yang, J.; Konegger, T.; Kleitz, F.; Thomas, A. A covalent organic framework/graphene dual-region hydrogel for enhanced solar-driven water generation. *J. Am. Chem. Soc.* **2022**, *144*, 3083−3090.

https://doi.org/10.1021/acsestengg.3c00278
ACS EST Engg. 2023, 3, 1966−1974